Analysis of shattered pellet injection experiments at ASDEX Upgrade

Paul Heinrich[*1], G. Papp[1], M. Bernert[1], M. Dibon[2], P. de Marné[1], S. Jachmich[2], M. Lehnen[2],
T. Peherstorfer[3], N. Schwarz[1], U. Sheikh[4], J. Svoboda[5], and the ASDEX Upgrade Team[a]

[1]*Max Planck Institute for Plasma Physics, Garching, Germany,* [2]*ITER Organization,*
St. Paul-lez-Durance, France, [3]*Vienna University of Technology, Vienna, Austria,* [4]*EPFL,*
Swiss Plasma Center (SPC), Lausanne, Switzerland, [5]*Institute of Plasma Physics of the CAS,*
Prague, Czech Republic, [a]*See the author list of* U. Stroth et al. 2022 Nucl. Fusion 62 042006.

Introduction   Plasma terminating disruptions pose a major challenge for tokamaks with high plasma current and stored energy. The foreseen disruption mitigation system (DMS) for ITER is based on massive material injection (MMI) in the form of shattered pellet injection (SPI) [1]. In late 2021, a highly flexible SPI system was installed at ASDEX Upgrade (AUG) to provide further input for the design and optimisation of the ITER DMS [2, 3]. In this contribution we focus on the radiation analysis of the 2022 AUG SPI experimental campaign.

Experimental setup   The AUG SPI is a triple-barrel system, where the main motivation is that the 3 independent guide tubes can be equipped with different shatter heads. Three pellets, made of mixtures of deuterium and neon can be generated and fired with high pressure gas simultaneously [4], potentially allowing the study of multi-injection scenarios. Following extensive laboratory commissioning and the analysis of fast camera recordings of the resulting pellet sprays [5], 3 different shatter heads (all with miter bends) were selected for the 2022 experimental campaign. A short, circular cross-section 25° head is used for increased spatial spread of the fragments. Two long, rectangular cross-section heads were installed for better collimation. These are a matching pair with shatter angles of 12.5° and 25° respectively, which allows the matching of the normal impact velocity – the main factor for the pellet fragment size distribution – at different parallel penetration speeds. In the 2022 campaign a total of ~240 discharges were allocated to SPI experiments.

Radiation asymmetries   In preparation for the SPI experiments, 5 new sets of absolutely calibrated 4-channel foil bolometers have been installed at 5 different toroidal locations inside ASDEX Upgrade (angle to sector of SPI - clockwise: S16 (0°), S15 (22.5°), S9 (157.5°), S5 (247.5° or −112.5°), and S1 (337.5° or −22.5°). Geometrical weighting factors are employed to calculate the radiated power in each sector. Figure 1 shows the time evolution of the plasma current and radiated power in each sector for AUG shot #40520.

Here, a single, 4 mm diameter, 1.25% neon pellet ($\sim 4.4 \times 10^{19}$ neon atoms) was injected. Due to the long pre-TQ (thermal quench) phase, 4 individual radiation peaks are visible in figure 1(b): The first, as the fragments enter the plasma; the second peak is likely connected to mixing events; the third around the TQ and IP-spike; and the last peak typically around $\sim 50\%$ of the current quench (CQ) potentially connected to the VDE-like final losses of the plasma.

Figure 1: *Up to 4 radiation peaks visible for long disruption phases.*

The toroidal asymmetry of the radiation – as visible in the first peak between the injection sector 16 and the other sectors – can be characterised by the toroidal peaking factor (TPF). For the plot in figure 2(c) the TPF is defined as the global maximum of the radiation divided by the mean of all 5 sectors at the same point in time. As shown in figure 2, the TPF reduces with increasing neon content and/or decreasing parallel velocity. Changing the pellet/shatter parameters or increasing the neon concentration, the plasma current quench in figure 2 transits from a convex (a), over linear (b) to a concave (d, e) shape. At the same time, the last radiation peak first reduces to a plateau-like shape and finally is absorbed into the single radiation peak. Potential fine structures may be smoothed by the sampling rate of 1 ms and temporal smoothing of the foil bolometers.
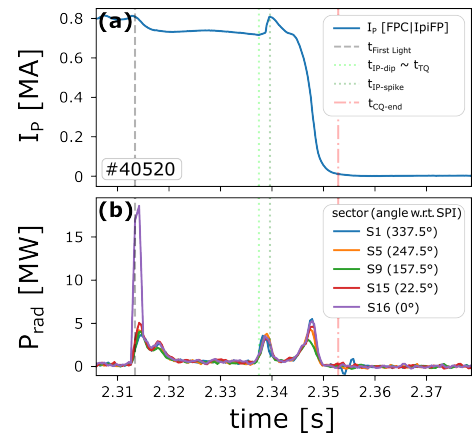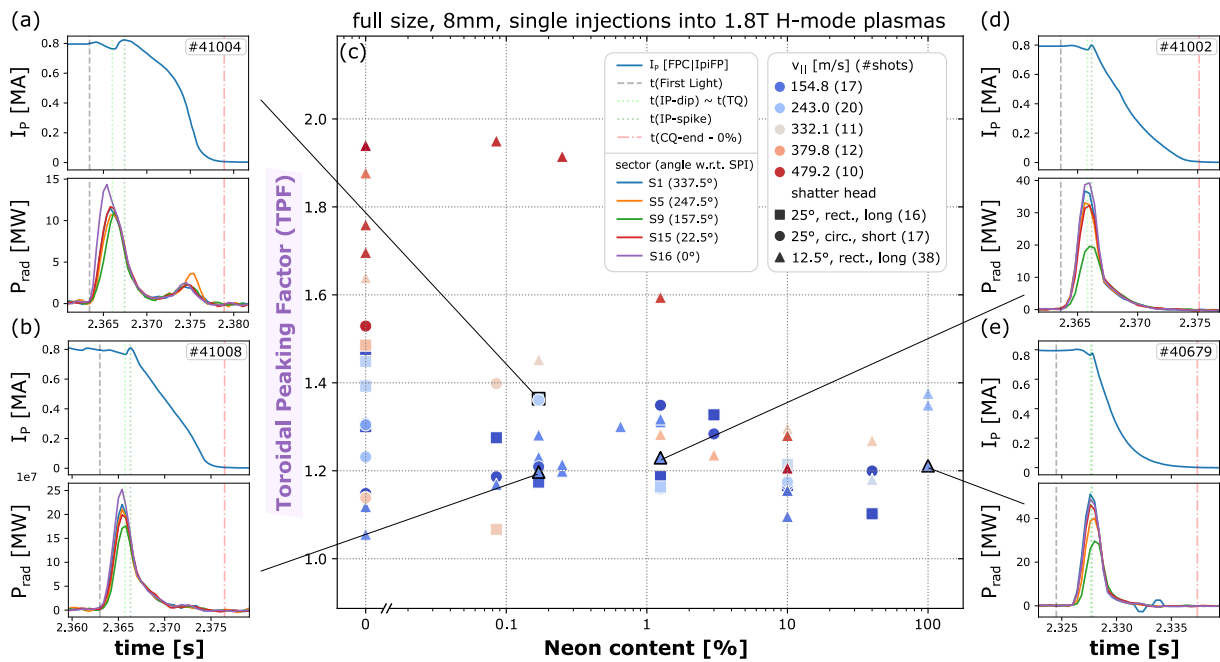

Figure 2: *TPF plotted against neon content as well as examples for the evolution of plasma current and radiation characteristics with pellet parameters.*

The highest asymmetries are observed for pure deuterium or low neon content pellets, where the total radiated power is low. Neon radiates strongly as it is (partially) ionized, hence, as it spreads toroidally along the field lines, while deuterium is expected to mainly radiate in the injection location in sector 16. Additionally a higher asymmetry was observed for higher fragment penetration velocities.

Radiated energy fraction   For an efficient disruption mitigation, it is desired that a high percentage of the plasma stored energy is radiated in an isotropic fashion. The pre-disruption energy stored inside the plasma can formally be divided into a magnetic and thermal component as given on the left side of the energy balance equation [6]

$$W_{th} + W_{mag} = W_{rad} + W_{coupled} + W_{cond} + W_{RE}.$$

During a disruption, the previously stored energy is released and can damage the device. Maximising the radiated energy fraction (f_{rad}) – within the given boundary conditions e.g. CQ times – is an important goal of the MMI mitigation schemes. For the energy that is not radiated, part of it will either couple into the surrounding structures (e.g. vessel, coils) which can lead to large vessel forces; or might generate a relativistic runaway electron (RE) beam. The remaining energy will be conducted to the plasma facing components (PFCs) which burdens the material and might cause melting. The radiated energy fraction is defined as

$$f_{rad} = \frac{W_{rad}}{W_{mag} + W_{th} - W_{coupled} + W_{heating}}, \tag{1}$$

which is ideally close to 1 for an efficient mitigation scheme. We expand the denominator in equation (1) with the term $+W_{heating}$, as Ohmic heating and the external heating sources – typically neutral beam injection (NBI) – still insert heat into the plasma during the disruption. For this contribution, full absorption of the energy is assumed. Based on massive gas injection (MGI) experiments at JET [6] and AUG [7], $W_{coupled} = 0.5 \cdot W_{mag}$ was chosen to calculate the coupled energies.

Figure 3 shows the radiated energy fraction after the injection of pellets with different neon concentrations and shatter parameters. In figure 3(a) the subset of full-size, 8 mm pellet diameter, single injections into the SPI standard 1.8 T H-mode is given. The data shows a strong dependence on the neon content and a weaker one on the shattering parameters (however, this depends on neon content). We observe a slight increase in f_{rad} with increased parallel velocity across the different neon concentrations; however, no obvious trend in f_{rad} was observed for
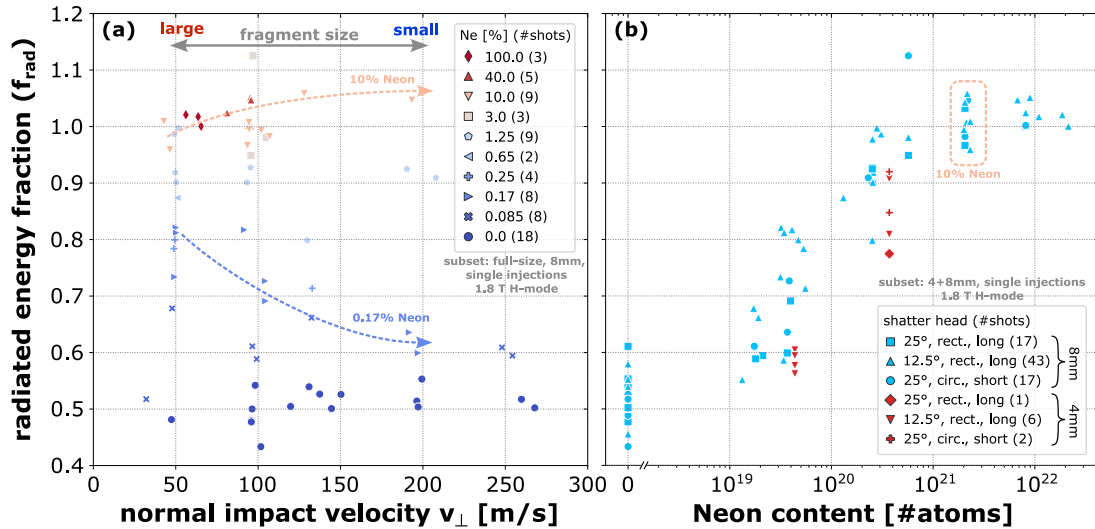
Figure 3: *(a) f_{rad} weakly depending on pellet/shatter parameters (fragment size depency depicted). (b) f_{rad} increases with the neon content. For large enough neon quantities, the shatter geometry and pellet size has only a small influence.*

other pellet- or shattering parameters (compare partially opposing trends for fragment size as displayed in figure 3(a)). In figure 3(b), f_{rad} is plotted as a function of the number of injected neon atoms. The dependence on the neon content dominates over the impact of the shatter head geometry – indicated by the marker styles – and pellet dimensions (length & size). The curve saturates around 2×10^{21} neon atoms (equals 10% neon for 8mm pellets), while the early CQ time (100-80%) continues to decrease exponentially with increasing neon content.

References

[1] M. Lehnen *et al.*, The ITER Disruption Mitigation System (...), TSDW Princeton (USA), 2021.

[2] M. Dibon *et al.*, Reviev of Scientific Instruments 94 043504, 2023.

[3] S. Jachmich *et al.* (this conference) O2.104 EPS 2023.

[4] P. Heinrich, ASDEX Upgrade SPI animation video https://datashare.mpcdf.mpg.de/s/DlMzGcWnZwoHMjq.

[5] T. Peherstorfer, Fragmentation analysis of cryogenic pellets for disruption mitigation, MSc, TU Wien, 2022.

[6] M. Lehnen *et al.*, Nuclear Fusion 53 093007, 2013.

[7] U. Sheikh *et al.*, Nuclear Fusion 60 126029, 2020.